Green Chemistry

PAPER

View Article Online
View Journal

Cite this: DOI: 10.1039/d6gc01091a

Boosting energy input and milling efficiency in a mixer mill with 3D-printed milling bodies

Tim Jansen, Daniel John Schmitz, Jovana Obradović and Carsten Bolm *

Received 20th February 2026,
Accepted 23rd April 2026

DOI: 10.1039/d6gc01091a

rsc.li/greenchem

Applying energy efficient, sustainable chemical methods is crucial to science and society. By minimising both solvent quantity and energy consumption, synthetic mechanochemistry shows a high potential in that respect. In industrial settings, this technique would benefit from targeted equipment maximising the energy input. Here, we designed, 3D-printed, and tested multiple new milling bodies with various geometries. Using a triboluminescent copper complex as indicator, high speed footage and time measurements allowed quantification of the milling efficiency of those milling bodies. Changing them from the commonly used milling balls to shapes, which corresponded better with the vessel geometries, like cylinders, improved the energy transfer and enhanced the overall milling efficiency by orders of magnitude. The results were confirmed by a representative organic reaction. The required equipment modifications are easily implemented and can reliably lower the energy consumption during mechanochemical synthesis.

Green foundation

1. This investigation takes the already green technology of mechanochemistry to a further step by introducing new milling body geometries which enhance the energy transfer. As a result, the milling machine has a lower energy consumption.
2. In this study, the particle size degradation of a triboluminescent copper complex served as an analytical tool. With the use of cylindrical milling bodies, the decay time of the light emission could be reduced to under 20% of the required time with a normal milling ball. This leads to less stress on the machines, as well as time and energy savings in the operational environment. The outcome of a representative organic reaction supported these observations.
3. Future research will be focused on the applicability of the new milling bodies in mechanochemical reactions with the vision to reduce external heating and the usage of milling auxiliaries.

Introduction

In recent years, mechanochemistry has become a well-recognised field with high appreciation for its simple operational procedures and attributes such as low energy consumption and the need for minimal solvent amounts. Instead of thermic energy as used in classical synthesis, mechanical energy derived from pressure, shearing, friction, and impacts drives reactions there. Compared to solvent-based counterparts, mechanochemistry provides synthetic methods with increased sustainability[1] and a high potential for a greener future.[2] The ability to perform reactions without solvents enables unique transformations and can even result in altered selectivities.[3] Although mechanochemistry has a long history,[4] there is still substantial potential for further research and technological improvements when it comes to synthetic applications. This is particularly true for scale-ups with the vision of potential industrial applications.[5] There, besides ball mills also other devices such as extruders and resonant acoustic mixers are considered for inducing reactivity.[6] In academic research with the focus on reaction discovery and optimization, mostly table-top shaker and laboratory planetary ball mills are used. Although there were many publications describing optimisations of these systems, either in theoretical or practical aspects, they mainly focus on certain variations, such as material and size of milling vessels and balls or amount of reactive material. More recently, also other points have been addressed including the use of additional forces like heat, light, ultrasonic sound, and electrical impulses.[7] Even though all these optimisation methods are valuable for the whole community, the equipment itself has remained essentially unaltered. Wondering about missed opportunities, we recently demonstrated that the geometry of the milling vessel has a major effect on the modes of action of the milling balls, which significantly impacts the milling efficiency.[8] In general, one can distinguish between a rolling mode, where pressure and shear forces are relevant, and a hitting mode, where impact forces dominate. In comparing the two, the latter leads to a higher energy transfer. Adjusting the vessel geometry allows to control both modes, which can be useful for significantly

Institute of Organic Chemistry, RWTH Aachen University, Landoltweg 1, 52074 Aachen, Germany. E-mail: Carsten.Bolm@oc.rwth-aachen.de

enhancing the energy output of the overall system.[8] Building on this prior work, we now investigated the effects of geometry variations of the milling bodies. All experiments were performed in a common mixer mill (Insolido IST 636) using high-speed camera mapping[9] and time-resolved measurements for analysing the behaviour of a triboluminescent copper complex as indicator.[8] In total, 24 new milling bodies were designed, 3D-printed, and tested inside of a 3D-printed vessel.

Results and discussion

Experimental setup

As shown before, the use of transparent vessels allows a direct observation of the movements of the milling bodies inside the vessel.[8–10] The number of energy dense impacts of the milling bodies with the vessel walls can be quantified and systematically investigated by measuring the emitted light flashes generated by the crystal breaking of triboluminent [Cu(NCS)$(py)_2(PPh_3)$][11] with the help of high-speed video recordings. This particular copper(I) complex (Fig. 1) was selected due to the high brightness of the emitted ice blue light and the synthetic ease to obtain it.[10] In all experiments, the same batch of triboluminescent crystals was used. Measuring the size of the crystals with sieves having varying hole diameters revealed the following distribution before the milling: ≥3.00 mm: 5%, 1.50 mm–3.00 mm: 21%, 1.00 mm–1.50 mm: 19%, 0.75 mm–1.00 mm: 22%, and <0.75 mm: 33%. The combination of directly observing the milling body motion inside the vessel while simultaneously identifying the contacts with the vessel walls can be applied in mapping energy densities. For this evaluation, single-frame analysis was used. The energy density of individual impacts can be determined by the emission of light, which corresponds to the minimum energy to fracture the crystalline complex. Hence, the milling bodies with more or broader flashes show more energy transfer from the milling bodies to the material.

Considering the emitted light wavelength of 426 nm, a red flashlight was used to illuminate the experimental setup providing sufficient light exposure for the high-speed footage to pick up the details of the moving parts (Fig. 2). The red light did not interfere with the capturing of the blue flashes, and thus, all the triboluminescent light emissions remained visible to the camera and could be mapped reliably during post-processing.

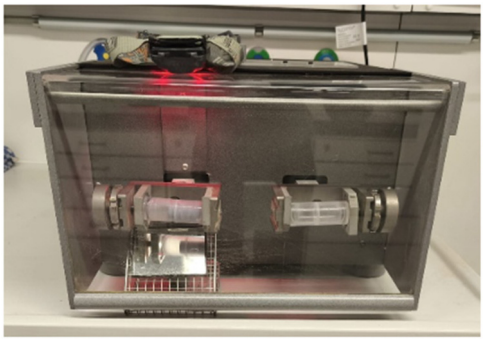

Fig. 2 Experimental setup for capturing high-speed footage. In an Insolido IST 636 mixer mill, a mirror was placed underneath to get a second point of view. A red flashlight was used to illuminate the setup.

To obtain an additional perspective, a mirror was placed underneath the captured milling arm, allowing simultaneous capturing of the view footage from the front and the bottom. The analysed data set consisted of six high-speed videos recorded at 960 frames per second, each covering a timeframe of half a second, which adds up to three seconds of mapped time in total. These videos were obtained by placing the high-speed camera (Samsung Galaxy S20Fe) in a tripod in front of the mill. For each video, the mill was started and after reaching the desired frequency, the video was captured. Then, the mill was stopped. After every second recording, the copper(I) complex was renewed to get a total of three loadings of 100 mg complex for each individual datapoint. For post-processing, the videos were transferred to a computer, and the frame was cut to only capture the vessel and its mirror image. The video was watched frame by frame to observe the flashes of light. These light flashes were mapped in an excel-designed raster map, where each hit within a specific square increased the hit count of this square by one, so that broader hits, which transferred more energy to the crystals, led to higher counts. After all hits were captured, the map was coloured to provide the "hit map". We were aware that for milling bodies showing the highest impact frequencies, this protocol could eventually lead to an underestimation of the actual hit counts due to a too rapid degradation of the complex.

However, this compromise between the two extremes – either renewing the copper complex after every video or using a single batch for all six videos – was considered acceptable for comparing all data points to each other within the given setup while retaining experimental practicability.

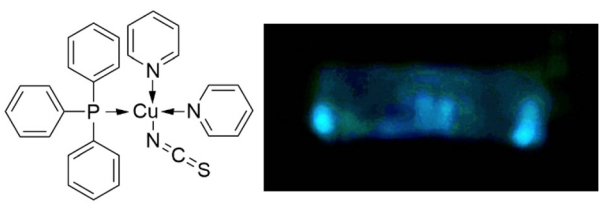

Fig. 1 [Cu(NCS)$(py)_2(PPh_3)$] (left) was used as triboluminescent crystal to create light flashes, as seen in the long exposure photograph (right). The long exposure was taken with an ISO50 and two seconds exposure time. In post-processing the picture was altered in contrast and brightness. The photo was taken at a frequency of 25 Hz and 100 mg of copper complex.

Analysis of the reference milling ball

For the analysis of the milling bodies, the hit-map of this vessel milling body combination was used. These maps represent the positions as well as the number of hits within the observed three-second timeframe. To create these hit maps, the inner geometry of the milling vessel was divided into multiple discrete sections. These sections were filled by analysing

the high-speed footage frame by frame and mapping the light flashes at the corresponding section within the vessel. Broader flashes will lead to a higher field coverage than small ones, therefore impact area as well as energy were considered, rather than hitting frequency only. Fig. 3 shows a hit map of the used 3D-printed jar (with a diameter of 19 mm and a height of 70 mm, printed with an Anycubic High Clear Resin, density: 1.05–1.12 g cm^{-3}, hardness: shore D77–79[12]), tested with a 3D-printed ball (with a diameter of 10 mm, printed with an Anycubic Tough Resin 2.0, density: 1.10–1.15 g cm^{-3}, hardness: shore D82–84[13]), at 25 Hz. This hit map serves as the reference point for all other milling body geometries, which will be discussed later.

Consistent with earlier investigations,[7] the hit map shows areas with higher hit counts and areas with lower hit counts. These can be explained by the different modes of action within shaker ball mill. The front view shows a concentration of hits at the ends and on distinct places in the middle of the jar vessel, which resemble the pathways of the milling ball. In contrast, the bottom view does not show a distinct pathway, but a slightly higher concentration of hits in the front half of the jar. This asymmetric distribution of hits arises from the centrifugal force, originating from a radial motion of the milling arms, which pushes the milling bodies towards the observer. This effect is underlined by the comparison of the obtained hit counts of the front view (462) and the bottom view (264), showing that 64% of all detected hits occurred in the front view. By using the complete time frame of three seconds within the high-speed footage, and therefore the large number of individually mapped impact events, the data are statistically relevant and comparable with other milling bodies.

Analysis of new milling bodies

With the hit map analysis as a powerful tool, the new milling bodies were analysed. 3D printing enabled the manufacturing of a wide variety of different milling body geometries. A general overview of these geometries without scaling is provided in Fig. 4. All milling bodies were printed with an Anycubic Tough Resin 2.0 (density: 1.10–1.15 g cm^{-3}, hardness: shore D82–84[13]), and complete specifications of them are available in the SI.

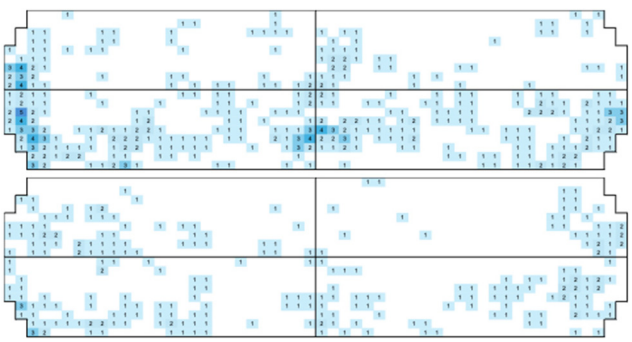

Fig. 3 Hit map of the 3D-printed milling jar with the reference milling ball. Top: Front view; bottom: bottom view.

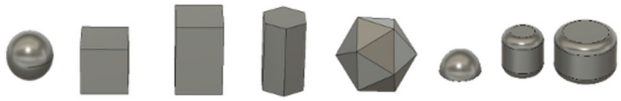

Fig. 4 New milling body geometries. From left to right: milling ball, cube, cuboid, hexagonal prism, icosahedron, half sphere, cylinder (diameter 10 mm), cylinder (diameter 15 mm). The milling bodies are not in scale, and technical drawings can be found in the SI.

The investigated milling bodies ranged from cubes in various sizes over cuboids, hexagonal prisms, an icosahedron, half spheres to cylinders in various dimensions. For those milling bodies, hit maps were prepared to enable quantitative comparison. The corresponding hit counts for selected milling bodies are shown in Fig. 5. (For a complete overview, see the SI.)

The pointy shapes generally performed worse than the reference milling ball. This behaviour can be explained by a lack of smooth, fluent motion while milling, leading to fewer impacts with the walls and therefore less emitted light. However, it is possible that the energy amount per hit could be comparable to or even higher than that of the milling ball, due to the smaller impact area within a cylindrical vessel. This localised concentration of impact energy cannot be properly measured with this method. Nevertheless, the significantly lower amount of hits shows that, even with this thought in mind, the overall energy transfer is less efficient with these shapes. The hemispherical milling body exhibited a comparable behaviour where the absence of a fluent motion hinders a high contact rate with the walls, although the hit area should play a less important role. In contrast, the cylindrical milling bodies performed significantly better. In particular, the cylinder with a height of 10 mm and a diameter of 15 mm was of interest, because it even exceeded the hit count of the reference milling ball by 27% reaching an overall hit count of 923. Based on these results, we continued investigating more cylindrical milling bodies with systematically varied heights.

Besides the aforementioned factors it is noteworthy that the milling bodies will be prone to different types of stress. The

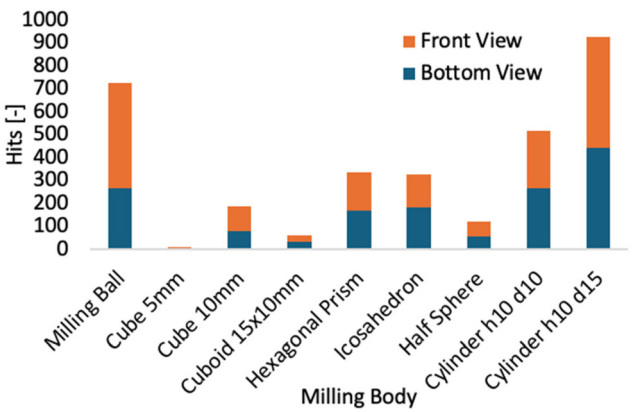

Fig. 5 Hit counts of the different milling bodies (at 25 Hz) as shown in Fig. 4. The hit counts represent the front view (orange) and the bottom view (blue).

one on the milling ball is distributed across its whole surface, whereas the pointy milling bodies encounter higher stress at their edges. In contrast to that, the stress on the cylinders is mainly on the rounded edges. If these stress factors become relevant to the milling vessels, the pointy shapes can lead to a damage of the vessel because of their high force-to-impact area ratio. The milling ball and the cylinders, on the other hand, distribute the force over a wider area.

Cylinders in various sizes

The promising results of the initial two cylinders led to the design and 3D printing of additional cylinders, which are described in the following by their dimensions with the method: height (h)[mm]–diameter (d)[mm] like in the following example: h10–d15. The results of the hit map counts are shown in Fig. 6.

The red line represents the hit count of the milling ball (726 hits) at a milling frequency of 25 Hz. All cylinders with a diameter of 15 mm exceeded this hit count number. Moreover, the cylinders with 10 mm diameter showed higher hit counts than the ball only if they were 20 mm in height and higher. The top hit counts were reached with the cylinders of 35 mm height, reaching up to 1′850 hits with the 10 mm cylinder and up to 3′176 hits with the 15 mm cylinder. A pronounced increase in hit numbers was observed between the height of 15 mm and 20 mm, which can be explained by the limitation of the degrees of freedom of movement within the milling jar. Given the inner diameter of the milling jar at 19 mm, the rotational motion is suppressed with increasing cylinder heights until reaching a point where no rotation is possible. This leads to predominantly translational motion, with parts of rotation around the *x*-axis and tilting along the *y*- and *z*-axes, as shown in Fig. 7.

Fig. 7 compares the free movement of the h15 mm cylinder with the tilting of the h25 mm cylinder and the emergence of dead volumes with the h45 mm cylinder. One advantage of the restriction of the degrees of freedom of movement is that less internal energy is dissipated to the rotational movement, allowing more velocity within the translational movement and therefore higher momentum and impact energies. Additionally, tilting at the rounded ends of the milling vessel leads to reliable secondary and tertiary hits (Fig. 8), which result in more energy transmission and thus a better milling efficiency.

Such effects are observed with the d15 mm diameter cylinders as well. The data in Fig. 6 indicate the existence of an optimum for the cylinder height, which is approximately at a height of 35 mm. Beyond, the hit counts decrease to even lower numbers than with the h20 mm cylinders. This decline in hit counts can be explained by the formation of dead volumes within the milling jars. Since the cavity inside of the milling jar has the dimensions of 19 mm diameter and 70 mm height, the cylinders of greater heights could only reach the middle of the jar, while completely flat, therefore creating areas with little to no interaction of the milling body with the milling vessel due to constant tilting. Moreover, if a flat contact occurs, the contact area is much higher and therefore

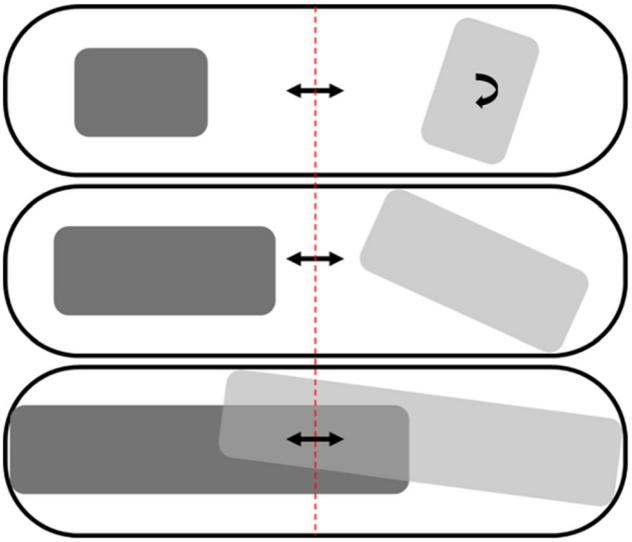

Fig. 7 Schematic drawing of the three regimes of movement with changing cylinder height. Free spinning over all axis with a h10–d15 cylinder (top). Limited rotational movement and tilting with a h25–d10 cylinder (middle). Emergence of dead volumes at the overlap with a h45–d10 cylinder (bottom).

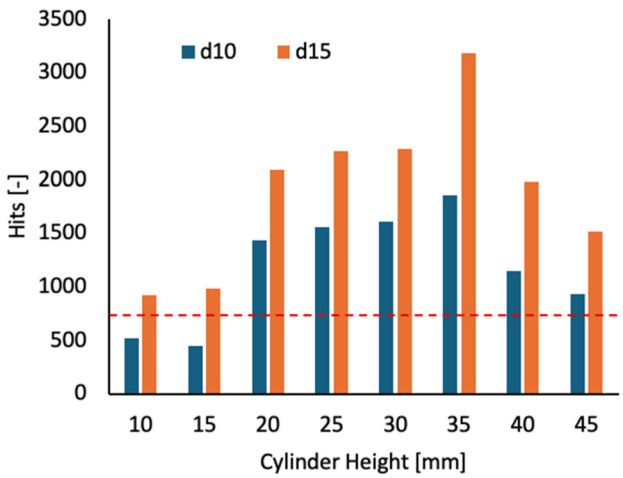

Fig. 6 Overall hit counts of the different cylinders, sorted by their diameter, 10 mm blue, 15 mm orange, and their height, let to right 10 mm to 45 mm in 5 mm steps.

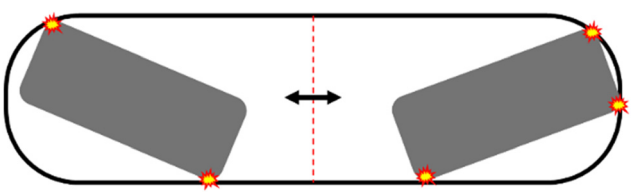

Fig. 8 Schematic view of secondary hits (left) and tertiary hits (right) due to tilting of a h25–d10 cylinder.

the force at impact significantly lower. As a result, the crystals may not break to emit light. *This leads to the conclusion that cylinders with approximately half the height of the inner height of the milling jar result in the highest hit counts*, although the movement patterns are equivalent beyond the point of rotational suppression. This can further be attributed to the higher volumes and therefore masses, and the greater surface areas of the bigger cylinders. The higher mass leads to stronger impacts due to relation between mass, velocity and force, whereas the higher surface area causes more possible contact area of the milling body and the wall. Together, these factors are the driving force for the superior performance of the d15 mm cylinders in comparison to the d10 mm cylinders.

Even though these results are promising for further investigations they must be considered with care. Because the stress on the milling bodies is proportional to the amount and force of hits that they experience, the best cylinders will endure more material stress in comparison to a normal milling ball. However, since the stress and the effectiveness of a milling body are linked, the higher number of hits per time could still compensate the higher stress amount and become valuable by shortening the milling times.

In summary, three distinct motion regimes could be observed with the cylindrical milling bodies: the first one is the free turning of the cylinders, where the movement around all axes was nearly unhindered, leading to low to medium amounts of total hits. The second regime is the hindered motion of the cylinders without dead volumes. Within this range, the best results were found with the highest hit numbers occurring when the cylinder was half the height of the vessel. The last regime is the emergence and widening of dead zones, where the hit counts drastically decreased again.

Frequency variations of selected cylinders

For getting a better overview of the potential applications in chemical reactions and possible energy savings, the cylinders h30–d10 and h30–d15 were tested at varying frequencies. The hit count data at varying frequencies showed that even at 15 Hz, the h30–d15 cylinder, resulting in 1′203 hits, performed 66% better than the milling ball at 25 Hz (726 hits). At 20 Hz, the h30–d10 cylinder hits (891) exceeded the number of the milling ball (726) as well. In general, the hit counts of the cylinders increased with frequency, which corresponded well with the increased external energy input into the system. These results indicate that the cylindrical milling bodies can increase the amount of hits, powerful enough to break the triboluminescent crystals, even with lower frequencies of the mill. This has important practical advantages, as lower operating frequencies reduce wear of the mill itself and additionally decreases energy consumption because of the lower acceleration of the mass of the milling parts. At a high level, however, the wear of the milling bodies and vessels may remain due to the significant number of powerful impacts. When thinking about normal working properties of shaker mills, the higher amount of hits at a given frequency should lead to both shorter reaction and milling times, thereby improving energy as well as time efficiency (Fig. 9).

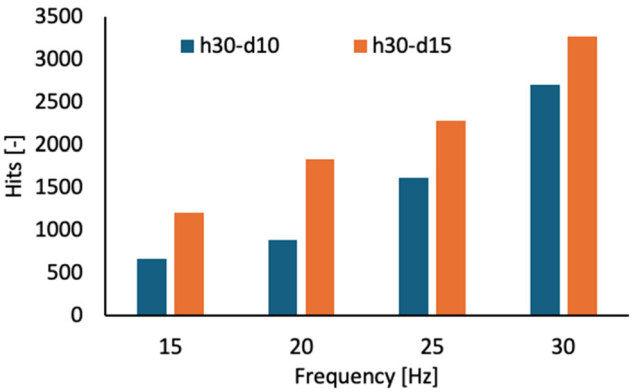

Fig. 9 Overall hit numbers of the h30–d10 (blue) and h30–d15 (orange) cylinders at milling frequencies of 15 to 30 Hz.

Milling time for deactivating light emissions (various shapes)

Since the triboluminescence of the copper complex relates to the particle size degradation, this phenomenon can be used to investigate the milling efficiency. The latter was evaluated by measuring the time until no light reflexes could be observed anymore, indicating a particle size at which no more fractures occurred. The experiments started by loading 50 mg of the copper complex together with the respective milling body into a transparent jar. In a fully darkened room, the mill and a stopwatch were started, and the time, until no further light emissions were observed anymore, was measured. Each measurement was done twice, and the results were averaged. Fig. 10 shows the data for various milling bodies.

The time measurements exhibited a clear correlation with the hit counts of the respective milling bodies, with only the 10 mm cube and the half sphere changing places. Notably, the h15–d10 cylinder showed milling times closer to those of the milling ball in comparison to the hit counts. As anticipated, the

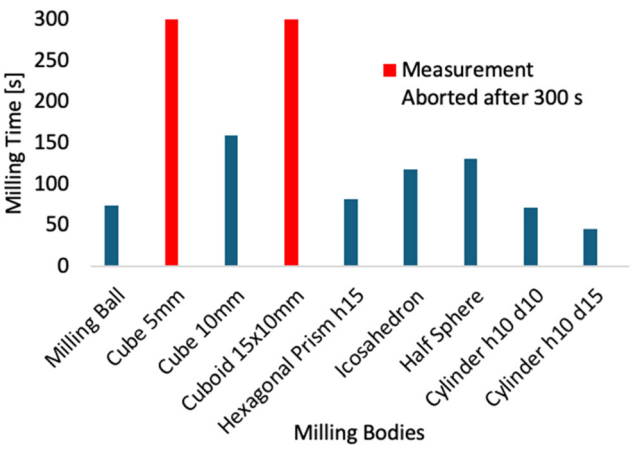

Fig. 10 Milling times until complete light decay with different milling body geometries. The measurements were done with 50 mg of the copper complex at a frequency of 25 Hz. The time until complete light decay was measured. With the 5 mm cube and the cuboid the measurements were terminated after 300 s.

milling times of the 5 mm cube and the cuboid were so long that the measurements were terminated after 300 seconds.

After these time measurements, the milling efficiency of the milling ball was evaluated by a particle size measurement. Thus, 50 mg of triboluminescent crystals and the milling ball were placed into the jar and the milling was done at 25 Hz for 74 s (time until complete light decay). Then, the powder was collected and analysed by sieving it with the 0.75 mm sieve. The result was that 72% of the mass of the retrieved powder were smaller than 0.75 mm. Apparently, a significant particle size reduction had occurred.

Milling time for deactivating light emissions (cylinders)

As revealed by the previous results, the cylinders of various heights achieved high hit numbers and outperformed the milling ball and the other milling bodies significantly. Thus, the light decay time for various cylinders was measured. The results are shown in Fig. 11.

Again, three distinct regimes were observed for the cylinders of different diameters. The first one, which can be observed with the h10–d10, the h10–d15, and the h15–d10 cylinders, corresponded to the free rotation over their height resulting in high milling times. (The h15–d15 cylinder could not be evaluated due to jamming after 10–20 seconds while the light emissions still occurred and the measurement proceeded. No other geometry showed such jamming, which is affected by many parameters such as angular velocity, hardness of the material, and size of both the cylinder and the milling jar. With harder materials like stainless steel the probability of jamming should be reduced even further.) In the second regime, which ranges from the h20 cylinders to the h35 cylinders, the milling time decreased sharply with increasing cylinder height. The best milling results were achieved with the h35 cylinders that showed light decays after 21.43 s and 13.6 s for the d10 and d15 cylinder, respectively. These results represent a drastic improvement in comparison to the time of the milling ball, which was at 73.22 s and therefore over 5 times longer than the milling time of the h35–d15 cylinder. Measuring the particle size with the 0.75 mm sieve after the experiment with the h35–d15 cylinder showed that 96% of the recovered particles were smaller than 0.75 mm. These results highlight the pronounced advantage of the cylinders over the standardized milling ball. Especially when choosing a cylinder of the right size, the same results can be achieved in a shorter timeframe. The third regime is, as for the hit counts, characterized by gradually increasing milling times, which corresponds to the hit counts. Therefore, the cylinders which fall into the first and third regime appear less effective. The cylinders within the second regime, however, are well suited for mechanochemistry and milling in general and should be implemented into mechanochemical synthesis.

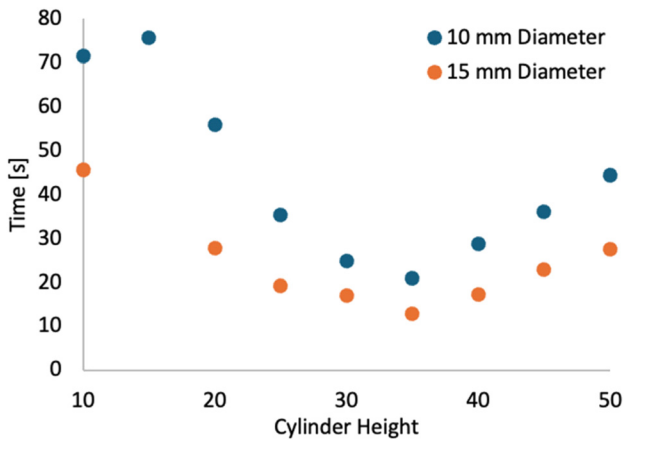

Fig. 11 Light decay measurements of the different cylinders. The cylinders are sorted by their diameter, 10 mm (blue) and 15 mm (orange) and their height, form 10 mm to 50 mm left to right. The measurements were done with 50 mg of the copper(I) complex at 25 Hz.

Evaluating the performance of the milling bodies in a mechano-chemical reaction

In order to confirm the observed increased milling efficiency by applying milling bodies with altered geometries, the study was extended by investigating a mechanochemical organic reaction. For this purpose, a nucleophilic substitution, originally reported my Mack and coworkers,[14] was used (Scheme 1).

The reaction was carried out with a milling ball and the two h35 cylinders (h35–d10 and h35–d15), which had led to excellent results in the milling time tests. For the analysis, ^{1}H NMR conversions were measured by comparing the CH_2 singlet of benzylbromide **1** with the CH_2 singlet of thiocyanate **2**. Although of limited accuracy, this method was fast and easy to perform providing first reference points for the performance of the milling bodies. Fig. 12 shows the results.

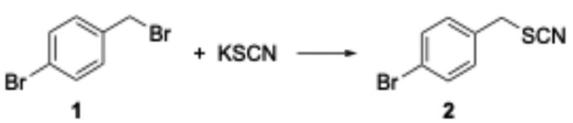

Scheme 1 Reaction of 4-bromobenzylbromide (**1**, 50.0 mg, 0.2 mmol) with potassium thiocyanate (58.3 mg, 0.3 mmol, 3 equiv.) to give 4-bromo-benzylthiocyanate (**2**).

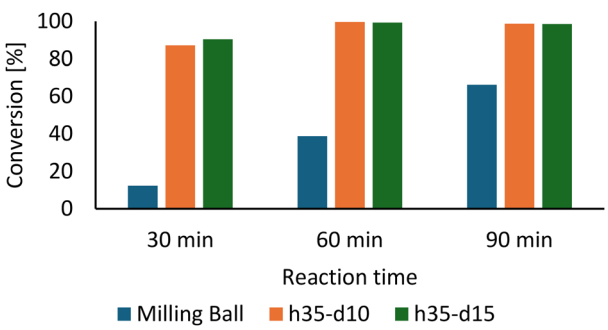

Fig. 12 NMR conversions of **1** to **2** in mechanochemical reactions at 25 Hz with a milling ball and the h35–d10 and h35–d15 cylinders after 30, 60, and 90 minutes.

As apparent from Fig. 12, a significant increase of the conversions of **1** to **2** was observed, when the milling ball was substituted by either of the two cylinders. For example, whereas the milling ball reached only a conversion of 66% after 90 min, the two h35 cylinders led to conversions of >85% within 30 min. After 90 min with NMR conversions were 99% with both cylinders. Thus, also the results from the test reaction illustrated the superiority of the cylinders over the milling ball leading to a consistent overall reactivity picture.

Conclusions

We tested new geometries of milling bodies and devised more energy efficient ways to operate shaker mills. The initial experiments were carried out by using a triboluminescent copper complex as indicator. The two ways of investigation were first, a visualisation and mapping approach, using a high-speed camera, and second, using the triboluminescence as direct indicator of particle size paired with time measurements. These two methods showed congruent results revealing rotational movement restrained cylinders as the best milling bodies. The cylinders are characterised by their diameter and their height, where the half of the inner height of the milling vessel caused the best results. With these cylinders the hit counts could be increased by 438%, and the milling time was decreased to under 20% of the time that a normal milling ball needed. These results were confirmed by studying the effect of cylinders in a nucleophilic substitution reaction where full conversions were achieved in significantly less time than with a normal milling ball. All these data highlight the importance of specialized milling bodies within mechanochemistry, with especially the cylinder geometries cutting milling times and lowering energy consumption.[15] A targeted use of those can therefore lead to a greener future.

Author contributions

T. Jansen, D. Schmitz, and J. Obradović performed the experiments and collected and analysed the data. T. Jansen and C. Bolm conceptualised and directed the project. T. Jansen wrote the original draft, and C. Bolm revised the manuscript. All authors have given approval to the final version of the manuscript.

Conflicts of interest

There are no conflicts to declare.

Data availability

The data supporting this article have been included as part of the supplementary information (SI). Supplementary information: technical drawings of the 3D prints; 3D printings of the designs; synthesis of the copper complex; imaging procedure and hit map creation; hit maps and hit counts of the milling body geometries; time measurements for particle size reduction; particle size measurements, the synthesis of 4-bromobenzylthiocyanate, and the results of the substitution reaction. See DOI: https://doi.org/10.1039/d6gc01091a.

Acknowledgements

This research was supported by the Deutsche Forschungsgemeinschaft (DFG, German Research Foundation) under Germany's Excellence Strategy – Exzellenzcluster 2186 "The Fuel Science Center" (ID: 390919832). The authors thank Michael Korfmacher for proofreading.

References

1 For selected reviews, see: (*a*) J. Breinsperger, N. Podlesnik, F. Mele and M. Schnürch, *Chem. – Eur. J.*, 2026, **32**, e03536; (*b*) J. Templ and L. Borchardt, *Angew. Chem., Int. Ed.*, 2025, **64**, e202503061; (*c*) A. Gallego, N. Pétry, J. Pinaud, O. Giani and F. Lamaty, *ChemistryOpen*, 2025, **14**, e202500232; (*d*) I. R. Speight, K. J. Ardila-Fierro, J. G. Hernández, F. Emmerling, A. A. L. Michalchuk, F. Garcia, E. Colacino and J. Mack, *Nat. Rev. Methods Primers*, 2025, **5**, 29; (*e*) M. Banerjee, A. Chatterjee, A. S. Aneja and A. Chatterjee, *J. Org. Chem.*, 2025, **90**, 5323–5335; (*f*) K. J. Ardila-Fierro and J. G. Hernández, *Angew. Chem., Int. Ed.*, 2024, **63**, e202317638; (*g*) F. Basoccu, L. De Luca and A. Porcheddu, *Eur. J. Org. Chem.*, 2024, e2024004; (*h*) J. F. Reynes, F. Leon and F. Garcia, *ACS Org. Inorg. Au*, 2024, **4**, 432–470; (*i*) N. Mukherjee, *Synlett*, 2024, 2331–2345; (*j*) E. Juaristi and C. G. Avila-Ortiz, *Synthesis*, 2023, 2439–2459; (*k*) I. d'Anciães, A. Silva, E. Bartalucci, C. Bolm and T. Wiegand, *Adv. Mater.*, 2023, **35**, 2304092; (*l*) M. T. J. Williams, L. C. Morrill and D. L. Browne, *ChemSusChem*, 2022, **15**, e202102157; (*m*) O. Bento, F. Luttringer, T. M. El Dine, N. Pétry, X. Bantreil and F. Lamaty, *Eur. J. Org. Chem.*, 2022, e202101516; (*n*) M. Xuan, C. Schumacher, C. Bolm, R. Göstl and A. Herrmann, *Adv. Sci.*, 2022, **9**, 2105497; (*o*) D. Virieux, F. Delogu, A. Procheddu, F. Garcìa and E. Colacino, *J. Org. Chem.*, 2021, **86**, 13885–13894; (*p*) T. Friščić, C. Mottillo and H. M. Titi, *Angew. Chem., Int. Ed.*, 2020, **59**, 1018–1029; (*q*) S. Mateti, M. Mathesh, Z. Liu, T. Tao, T. Ramireddy, A. M. Glushenkov, W. Yang and Y. I. Chen, *Chem. Commun.*, 2021, **57**, 1080–1092; (*r*) A. Porcheddu, E. Colacino, L. de Luca and F. Delogu, *ACS Catal.*, 2020, **10**, 8344–8394; (*s*) M. Pérez-Venegas and E. Juaristi, *ACS Sustainable Chem. Eng.*, 2020, **8**, 8881–8893; (*t*) W. Pickhardt, S. Grätz and L. Borchardt, *Chem. – Eur. J.*, 2020, **26**, 12903–12911; (*u*) K. Kubota and H. Ito, *Trends Chem.*, 2020, **2**, 1066–1081; (*v*) I. N. Egorov, S. Santra, D. S. Kopchuk, I. S. Kovalev, G. V. Zyryanov, A. Majee, B. C. Ranu, V. L. Rusinov and O. N. Chupakhin, *Green*

Chem., 2020, **22**, 302–315; (*w*) C. Bolm and J. G. Hernández, *Angew. Chem., Int. Ed.*, 2019, **58**, 3285–3299; (*x*) E. Colacino, A. Porcheddu, C. Charnay and F. Delogu, *React. Chem. Eng.*, 2019, **4**, 1179–1188; (*y*) J. L. Howard, Q. Cao and D. L. Browne, *Chem. Sci.*, 2018, **9**, 3080–3094; (*z*) J. G. Hernández and C. Bolm, *ChemSusChem*, 2018, **11**, 1410–1420; (*aa*) D. Tan and T. Friščić, *Eur. J. Org. Chem.*, 2018, 18–33; (*ab*) D. Tan, L. Loots and T. Friščić, *Chem. Commun.*, 2016, **52**, 7760–7781; (*ac*) S. L. James, C. J. Adams, C. Bolm, D. Braga, P. Collier, T. Friščić, F. Grepioni, K. D. M. Harris, G. Hyett, W. Jones, A. Krebs, J. Mack, L. Maini, A. G. Orpen, I. P. Parkin, W. C. Shearouse, J. W. Steed and D. C. Waddell, *Chem. Soc. Rev.*, 2012, **41**, 413–447; (*ad*) A. Bruckmann, A. Krebs and C. Bolm, *Green Chem.*, 2008, **10**, 1131–1141; (*ae*) B. Rodriguez, T. Rantanen, A. Bruckmann and C. Bolm, *Adv. Synth. Catal.*, 2007, **349**, 2213–2233.

2 (*a*) F. Gomollón-Bel, *Chem. Int.*, 2019, **41**, 12–17; (*b*) K. J. Ardila-Fierro and J. G. Hernández, *ChemSusChem*, 2021, **14**, 2145–2162; (*c*) N. Fantozzi, J.-N. Volle, A. Porcheddu, D. Virieux, F. Garcia and E. Colacino, *Chem. Soc. Rev.*, 2023, **52**, 6680–6731; (*d*) J. Alić, M.-C. Schlegel, F. Emmerling and T. Stolar, *Angew. Chem., Int. Ed.*, 2024, **63**, e202414745; (*e*) E. P. T. Leitão, *RSC Sustainability*, 2024, **2**, 3655–3668.

3 (*a*) J. G. Hernández and C. Bolm, *J. Org. Chem.*, 2017, **82**, 4007–4019; (*b*) J. L. Do and T. Friscic, *ACS Cent. Sci.*, 2017, **3**, 13–19; (*c*) F. Cuccu, L. De Luca, F. Delogu, E. Colacino, N. Solin, R. Mocci and A. Porcheddu, *ChemSusChem*, 2022, **15**, e202200362.

4 (*a*) L. Takacs, *Chem. Soc. Rev.*, 2013, **42**, 7649–7659; (*b*) M. Marchini, G. Montanari, L. Cesali, M. Martelli, L. Ragetti, M. Baláž, P. Baláž and L. Maini, *RSC Mechanochem.*, 2024, **1**, 123–129; (*c*) T. Stolar, J. Alić, L. Casali, N. Gugin, M. Baláž, A. A. L. Michalchuk and F. Emmerling, *Chem*, 2026, **12**, 102880; (*d*) A. Alamiery, *Discover Chem.*, 2026, **3**, 65.

5 (*a*) J. F. Reynes, V. Isoni and F. Garcia, *Angew. Chem., Int. Ed.*, 2023, **62**, e202300819; (*b*) S. Triller, F. Winkelmann, J.-H. Schöbel and M. Felderhoff, *RSC Mechanochem.*, 2025, **2**, 538–543; (*c*) L. Borchardt and S. Grätz, in *Handbook of Chemical Reactors*, ed. W. Reschetilowski, Springer Nature, 2026, pp. 1143–1169.

6 For representative overviews, see: (*a*) A. A. L. Michalchuk and E. V. Boldyreva, in *Reference Module in Chemistry, Molecular Sciences and Chemical Engineering*, Elsevier, 1st edn, 2024, DOI: 10.1016/B978-0-443-15742-4.00121-6; (*b*) P. Freisa, L. Lattuada, A. Barge and G. Cravotto, *RSC Mechanochem.*, 2026, **3**, 144–160.

7 For examples of optimisations and kinetic analyses of mechanochemical transformations, see: (*a*) M. Alrbaihat, F. K. Al-Zeidaneen and Q. Abu-Afifeh, *Mater. Today: Proc.*, 2022, **65**, 3651–3656; (*b*) K. S. Venkataraman and K. S. Narayanan, *Powder Technol.*, 1998, **96**, 190–201; (*c*) T. Kozawa, K. Fukuyama, K. Kushimoto, S. Ishihara, J. Kano, A. Kondo and M. Naito, *Sci. Rep.*, 2021, **11**, 210; (*d*) O. V. Lapshin, E. V. Boldyreva and V. V. Boldyrev, *Russ. J. Inorg. Chem.*, 2021, **66**, 433–453; (*e*) A. Politov and O. Golyazimova, *Faraday Discuss.*, 2014, **170**, 345–356; (*f*) S. Garrido Nuñez, D. L. Schott and J. T. Padding, *Powder Technol.*, 2025, **457**, 120919; (*g*) L. Vugrin, M. Carta, S. Lukin, E. Meštrovic, F. Delogu and I. Halasz, *Faraday Discuss.*, 2023, **241**, 217–229; (*h*) Z. Chen, S. Lu, Q. Mao, A. Buekens, Y. Wang and J. Yan, *Environ. Sci. Pollut. Res.*, 2017, **24**, 24562–24571; (*i*) V. Martinez, T. Stolar, B. Karadeniz, I. Brekalo and K. Užarević, *Nat. Rev. Chem.*, 2023, **7**, 51–65.

8 T. Jansen, L. C. Thomas and C. Bolm, *ChemSusChem*, 2026, **19**, e202502452.

9 For other examples of high-speed camera applications in ball mills, see: (*a*) S. Rosenkranz, S. Breitung-Faes and A. Kwade, *Powder Technol.*, 2011, **212**, 224–230; (*b*) K. J. Ardila-Fierro, S. Lukin, M. Etter, K. Užarević, I. Halasz, C. Bolm and J. G. Hernández, *Angew. Chem., Int. Ed.*, 2020, **59**, 13458–13462; (*c*) M. F. Rappen, J. Mäder, S. Grätz and L. Borchardt, *RSC Mechanochem.*, 2026, **3**, 235–242.

10 M. F. Rappen, L. Beissel, J. Geisler, S. T. Tietmeyer, S. Grätz and L. Borchardt, *RSC Mechanochem.*, 2024, **1**, 336–392.

11 (*a*) C. Pettinari, C. Di Nicola, F. Marchetti, R. Pettinari, B. W. Skelton, N. Somers, A. H. White, W. T. Robinson, M. R. Chirotti, R. Gobetto and C. Nervi, *Eur. J. Inorg. Chem.*, 2008, 1974–1984; (*b*) F. Marchetti, C. Di Nicola, R. Pettinari, I. Timokhin and C. Pettinari, *J. Chem. Educ.*, 2012, **89**, 652–655; (*c*) A. İncel, C. Varlikli, C. D. McMillen and M. M. Demir, *J. Phys. Chem.*, 2017, **121**, 11709–11716; For a review, see: (*d*) A. Szukalski, A. Kabanski, J. Goszyk, M. Adaszynski, M. Kaczmarska, R. Gaida, M. Wyskiel and J. Mysliwiec, *Materials*, 2021, **14**, 7142.

12 https://cdn.shopify.com/s/files/1/0698/1235/5357/files/ANYCUBIC-TDS-High_Clear_Resin.pdf?v=1757582959.

13 https://cdn.shopify.com/s/files/1/0245/5519/2380/files/ANYCUBIC-TDS-Tough_Resin_2.0_ba1eedb4-f8af-47d4-9102-8c2bfadade62.pdf?v=1758253760.

14 P. Vogel, S. Figueira, S. Muthukrishnan and J. Mack, *Tetrahedron Lett.*, 2009, **50**, 55–56.

15 For a recent related study employing hollow and solid balls as well as cylindrical and round-ended milling bodies, see: M F. Rappen, J. Mäder, T. Schwemin, S. Grätz and L. Borchardt, *RSC Mechanochem.*, 2026, **3**, 235–242.